

Quantum phase with coexisting localized, extended, and critical zones

Yucheng Wang^{1,2,3}, Long Zhang⁴, Wei Sun,⁵ Ting-Fung Jeffrey Poon,^{6,7} and Xiong-Jun Liu^{6,7,1,*}

¹*Shenzhen Institute for Quantum Science and Engineering, Southern University of Science and Technology, Shenzhen 518055, China*

²*International Quantum Academy, Shenzhen 518048, China*


³*Guangdong Provincial Key Laboratory of Quantum Science and Engineering, Southern University of Science and Technology, Shenzhen 518055, China*

⁴*School of Physics and Institute for Quantum Science and Engineering, Huazhong University of Science and Technology, Wuhan 430074, China*

⁵*Department of Physics, Southern University of Science and Technology, Shenzhen 518055, China*

⁶*International Center for Quantum Materials, School of Physics, Peking University, Beijing 100871, China*

⁷*Collaborative Innovation Center of Quantum Matter, Beijing 100871, China*

 (Received 20 February 2022; revised 31 July 2022; accepted 19 October 2022; published 27 October 2022)

Conventionally a mobility edge (ME) marks a critical energy that separates two different transport zones where all states are extended and localized, respectively. Here we propose a quasiperiodic spin-orbit coupled lattice model with experimental feasibility to realize a quantum phase with three coexisting energy-dependent zones, i.e., the extended, critical, and localized zones, and uncover the underlying generic mechanism for the occurrence of this quantum phase. Accordingly, this phase exhibits types of MEs which separate the extended states from critical ones and the localized states from critical ones, respectively. We introduce the diagnostic quantities to characterize and distinguish the different zones and show that the predicted phase can be detected by measuring the fractal dimension or conductivities. The experimental realization is also proposed and studied. This work extends the concept of ME and enriches the quantum phases in disordered systems, which sheds light on searching for localization and critical phenomena with transport and thermoelectric effects.

DOI: [10.1103/PhysRevB.106.L140203](https://doi.org/10.1103/PhysRevB.106.L140203)

Introduction. Disordered potential is ubiquitous in quantum materials and, as Anderson envisioned, can induce exponentially localized electronic wave functions when the randomness is sufficiently strong [1]. This implies the existence of disorder-driven Anderson transition (AT) between extended and localized phases [2–4]. The AT may also appear versus eigenenergies in a single phase in the moderate disorder strength regime, namely, a part of the states are localized and the rest are extended, with the localized and extended zones being separated by critical energies called mobility edges (MEs) [2]. A typical situation is illustrated in Fig. 1(a), with E_{c1} and E_{c2} denoting the MEs, where the states in band tails are localized, while those in the center remain extended. The AT can also be obtained in quasiperiodic lattices [5–17], in which the quasiperiodic potential has important difference from the random disorders. In particular, the AT and ME can exist in one-dimensional (1D) quasiperiodic systems [5–17], but in a disordered system they only exist in a dimension higher than two according to the scaling theory [18,19]. Quasiperiodic systems can be realized in ultracold gases by using two optical lattices with incommensurate wavelengths [20], with which the AT and ME have been observed recently in experiments [20–23].

The quasiperiodic systems can also host a third type of phase called critical phases [24–27], which are extended but nonergodic [10,15,28–31] and are fundamentally different from the extended and localized phases in the spectral statistics [32–34], multifractal properties of wave functions [35,36], and dynamical evolutions [37,38]. In the presence of interactions, the single-particle critical phase can become the many-body critical phase [17,39,40]. The critical phase is a fertile ground to explore various important physics such as the nonergodic physics, critical transport behavior, AT, and thermal-nonthermal transitions [41–44]. An important open question is whether a finite critical zone exists between the extended and localized zones in a single phase. Namely, is there a quantum phase with three coexisting fundamentally different zones with all eigenstates in one zone having the same properties, as illustrated in Fig. 1(b)? Presumably such a phase, if existing, shall host other quantum physics including different types of energy-dependent transport features (ballistic, normal diffusive, and localized), quantum dynamics, and thermoelectric response [11,45–50], which could be observed in experiment by tuning Fermi energy. Therefore, to uncover a system with three different coexisting energy-dependent transport zones is of both fundamental importance and potential applications, but was not considered before.

In this Letter, we predict a quantum phase with coexisting localized, extended, and critical zones in a 1D quasiperiodic model, which can be realized in current experiments, and

*Corresponding author: xiongjunliu@pku.edu.cn

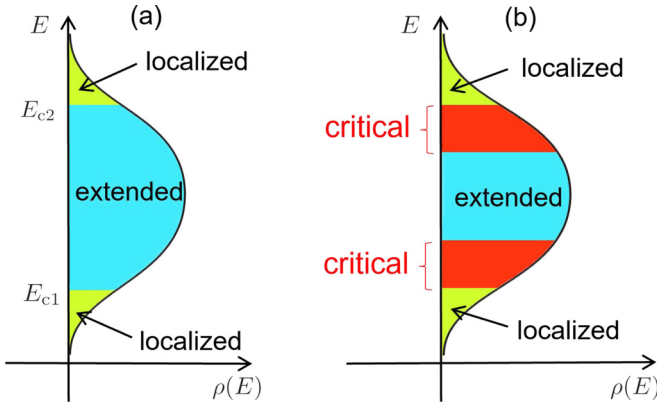


FIG. 1. Schematic figures of the density of states $\rho(E)$ versus the energy E for a system with (a) conventional MEs separating the extended and localized states and (b) three different energy-dependent transport zones (extended, critical, and localized) separated by the other type of MEs.

uncover the underlying generic mechanism for the coexisting phase. This phase exhibits two types of MEs separating the extended and localized zones from critical zones, respectively, with diagnostic quantities being introduced to characterize this phase.

Model and phase diagram. We propose the quasiperiodic optical Raman lattice model described by

$$H = H_t + H_{\text{SOC}} + H_Z, \quad (1)$$

with

$$H_t = -t_0 \sum_{(i,j)} (c_{i,\uparrow}^\dagger c_{j,\uparrow} - c_{i,\downarrow}^\dagger c_{j,\downarrow}), \quad (2a)$$

$$H_{\text{SOC}} = t_{so} \sum_i (c_{i,\uparrow}^\dagger c_{i+1,\downarrow} - c_{i,\downarrow}^\dagger c_{i-1,\uparrow}) + \text{H.c.}, \quad (2b)$$

$$H_Z = \sum_i \delta_i (n_{i,\uparrow} - n_{i,\downarrow}) + \lambda \sum_i \delta_i (n_{i,\uparrow} + n_{i,\downarrow}), \quad (2c)$$

where $c_{j,\sigma}$ ($c_{j,\sigma}^\dagger$) is the annihilation (creation) operator for spin $\sigma = \uparrow, \downarrow$ at lattice site j and $n_{j,\sigma} = c_{j,\sigma}^\dagger c_{j,\sigma}$ is the particle number operator, the term H_t (H_{SOC}) denotes the spin-conserved (spin-flip) hopping coupling between neighboring sites with strength t_0 (t_{so}), and the last term H_Z includes spin-dependent and spin-independent quasiperiodic potentials of strengths M_z and λM_z , respectively, with $\delta_j = M_z \cos(2\pi\alpha j + \phi)$ and α (ϕ) being an irrational number (a phase shift). This system with uniform Zeeman energy, i.e., $\delta_i = m_z$, and $\lambda = 0$ gives the 1D AIII class topological insulator and is experimentally realized [51–54]. For convenience, we set $t_0 = 1$ as the unit energy, $\phi = 0$, and $\alpha = \lim_{m \rightarrow \infty} \frac{F_{m-1}}{F_m} = (\sqrt{5} - 1)/2$, with F_m being the Fibonacci numbers [55,56]. For finite system with size $L = F_m$ one takes $\alpha = \frac{F_{m-1}}{F_m}$ to ensure the periodic boundary condition (PBC), and we use PBC unless otherwise stated.

To characterize the key physics of the above model, we define a characteristic quantity by

$$\kappa = \frac{N_e}{N} \times \frac{N_c}{N} \times \frac{N_l}{N}, \quad (3)$$

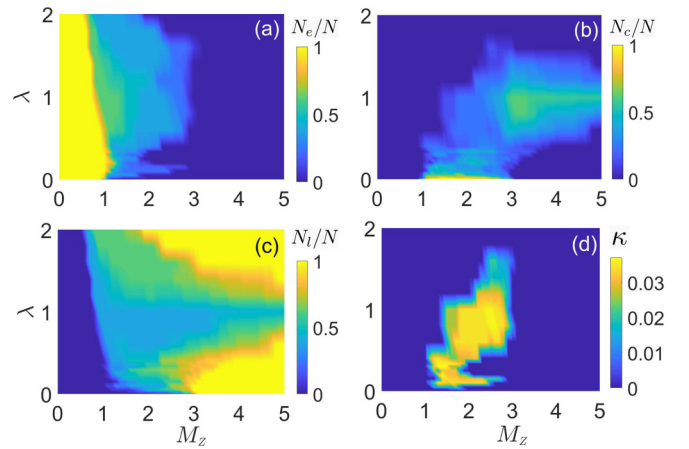


FIG. 2. (a) Extended fraction N_e/N , (b) the critical fraction N_c/N , (c) the localized fraction N_l/N , and (d) κ as the function of λ and M_z with $t_{so} = 0.5$.

where N_e , N_c , N_l , and $N = 2L$ are the numbers of the extended, critical, localized, and total eigenstates, respectively, providing the diagnostic quantities of all different phases. The conventional ME separating localized and extended states corresponds to $N_e N_l / N^2 > 0$ with $\kappa = 0$, while $N_e N_c / N^2 > 0$ (or $N_c N_l / N^2 > 0$) characterizes a type of ME separating critical states from extended (or localized) ones. The most nontrivial phase corresponds to $\kappa > 0$, which characterizes the coexisting localized, extended, and critical zones. Figure 2 show the $N_{e,c,l}/N$ and κ , which are calculated by comparing the fractal dimension (FD) with different sizes (see below). When $\lambda = 0$, this system hosts three distinct phases with solely extended ($N_e/N = 1$), critical ($N_c/N = 1$), or localized ($N_l/N = 1$) eigenstates [17]. However, with increasing λ to be within a proper range, a phase emerges with three coexisting zones and $\kappa > 0$ [Fig. 2(d)]. This phase occurs in a wide range of parameters about $0.02 < \lambda < 1.6$ for $t_{so} = 0.5$ [see Supplemental Material (SM) [57]]. Thus the presence of both spin-independent and spin-dependent quasiperiodic potentials, with strength λ being freely adjustable in experiment (see below), is terribly important for the coexisting phase, whose occurrence deeply stems from breaking chiral symmetry of this incommensurate AIII class system [57]. This key ingredient marks the fundamental difference in comparison with the previous study [17].

To further confirm the existence of this phase, we present a quantitative study with $\lambda = 1/3$. The different types of states can be identified by the FD Γ and, for an arbitrary state $|\psi\rangle = \sum_{j,\sigma} u_{j,\sigma} c_{j,\sigma}^\dagger |0\rangle$, it is defined as

$$\Gamma = - \lim_{L \rightarrow \infty} \ln(IPR) / \ln L, \quad (4)$$

where $IPR = \sum_{j,\sigma} u_{j,\sigma}^4$ is the inverse participation ratio [2]. The FD tends to 1 and 0 for the extended and localized states, respectively, while $0 < \Gamma < 1$ for the critical states. Figure 3(a) shows Γ of different eigenstates as a function of M_z and the corresponding eigenvalues E , from which one identifies the phase regions with coexisting three or two different types of eigenstates separated by MEs. Particularly, we fix $M_z = 1.5$, which belongs to the coexisting region of

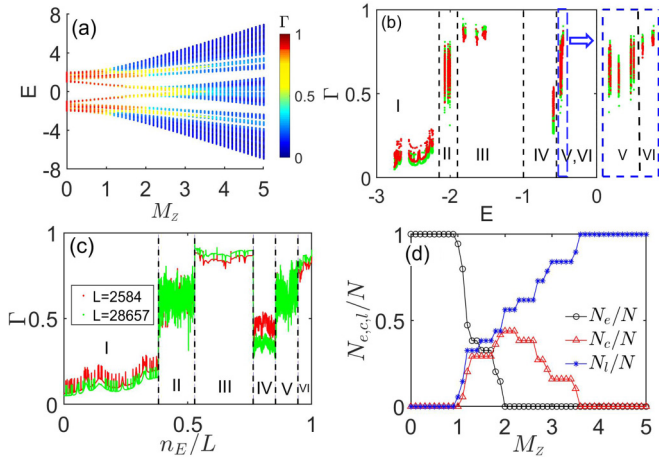


FIG. 3. (a) Fractal dimension Γ of different eigenstates as the function of the corresponding eigenvalues E and M_z with size $L = F_{14} = 610$. (b) Γ of different eigenstates versus the corresponding eigenvalues E for different sizes $L = F_{17} = 2584$ (red) and $L = F_{22} = 28657$ (green) with $M_z = 1.5$. The right blue dashed frame is the enlarged part of the left blue dashed frame. (c) Compared to (b), the horizontal axis becomes n_E/L with n_E being the index of energy mode. (d) N_e/N , N_c/N , and N_l/N as a function of M_z . Other parameters are $t_{so} = 0.5$, $\lambda = 1/3$.

extended, critical, and localized zones, and show Γ of different eigenstates in Fig. 3(b) as a function of the corresponding eigenvalues for different sizes. For convenience, we present the region with $E < 0$, which is symmetric to that with $E > 0$. One can observe that Γ tends to 0 for all states in zones I and IV with increasing the system size, implying that they are localized, while Γ tends to 1 for all states in zones III and VI when increasing the size, showing that all states are extended. In contrast, in zones II and V, the FD Γ is clearly different from 0 and 1 and, peculiarly, is almost independent of the system size, meaning that all states are critical. To distinguish different zones more easily, one can use the ratio of the index of energy mode n_E to L as the horizontal axis, instead of the eigenvalue E , as shown in Fig. 3(c). We see the distinguishable zones and the sudden change between different zones. More rigorously, in SM [57] and the following discussion about the momentum-space distributions, we study the scaling behavior of different zones and further confirm the coexisting phase. After determining the energy windows of extended, critical, and localized zones, one can easily compute numerically N_e/N , N_c/N , N_l/N , which are size independent [57] and can also be directly obtained from Fig. 3(c) [58]. Figure 3(d) displays the three quantities, for $1 < M_z < 2$, which are all larger than 0, signifying the phase with three coexisting zones.

Before proceeding we point out the generic underlying mechanism of the coexisting phase, with which we show that this phase can exist in a broad range of quasiperiodic systems. As detailed in SM [57], the current model with nonzero λ but zero spin-orbit coupling $t_{so} = 0$ has ME separating extended and localized states. On the other hand, the model with $\lambda = 0$ hosts critical phase [17]. The appropriate combination of the way to induce mobility edge and the way to induce critical phase gives rise to the coexisting phase. There are various

schemes to obtain mobility edges, such as the quasiperiodic systems with the next-nearest-neighbor [7], exponential [8], or power-law hopping [10] term, or multiple potentials [12,13]. Combining either of them with the way to induce critical phase can yield the coexisting phase. As we confirm in the SM, instead of considering spin-independent quasiperiodic potential (i.e., $\lambda = 0$), when a next-nearest-neighbor hopping term is added, or if the long-range hopping is present, the coexisting phase can also be readily obtained. These results show that this coexisting phase can be naturally realized in various quasiperiodic models in real condensed matter and cold atom systems.

Detecting three different zones. The detection of the three different characteristic zones can be achieved by contrasting the distribution of the wave functions in real and momentum spaces. The momentum distribution is defined as $n(k) = n_\uparrow(k) + n_\downarrow(k)$ for an eigenstate $|\psi\rangle$, where $n_\sigma(k) = \langle \psi | c_{\sigma,k}^\dagger c_{\sigma,k} | \psi \rangle$ and $c_{\sigma,k} = (1/\sqrt{L}) \sum_l e^{ikl} c_{\sigma,l}$. The distributions of localized (extended) states are localized (extended) in real space but extended (localized) in momentum space [see the red (blue) lines in Figs. 4(a) and 4(b)]. However, for the critical states the distributions are delocalized and nonergodic in both real and momentum spaces [see the black lines in Figs. 4(a) and 4(b)]. These qualitatively distinct features characterize and can be applied to detect different zones.

The momentum distribution of a quantum gas can be readily measured with time of flight imaging. Analog to the FD in real space, we introduce the IPR in momentum space $IPR(k) = \sum_{k_m, \sigma} n_{k_m, \sigma}^2$ with $k_m = \pi \frac{m}{L}$ ($m = -L, -L+1, \dots, L-1$) and define the FD $\Gamma(k) = -\lim_{L \rightarrow \infty} \ln[IPR(k)] / \ln L$. Since the momentum distributions are delocalized for the critical and localized states, to distinguish them, we utilize their different tendencies through the previous finite-size effect. But when varying the system size, the magnitudes and number of the eigenenergies may change accordingly. To avoid the potential challenge in contrasting $\Gamma(k)$ for a fixed state at different sizes, it is convenient to observe the average value over the eigenstates in a single zone, and accordingly we define the zone FD

$$\overline{\Gamma(k)} = \frac{1}{N_s} \sum_{\text{same zone}} \Gamma(k), \quad (5)$$

where N_s is the number of states of the zone, i.e., $\overline{\Gamma(k)}$ is obtained by calculating the average $\Gamma(k)$ of all states in the same zone. We note that since all eigenstates in the same zone have the same properties, the mean FD in an arbitrary small subzone of a zone can also be similarly defined and will show the same scaling behavior with the zone [59]. Figures 4(c) and 4(d) respectively show the $\Gamma(k)$ and $\overline{\Gamma(k)}$; we see that they extrapolate to 0 in zones III and VI and to 1 in zones I and IV, while to the values far from 0 and 1 in zones II and V, which confirms that the corresponding states in these zones are extended, localized, and critical in momentum space, respectively.

Ultracold atom experiments consisting of a channel connecting two reservoirs have been used to investigate and detect interesting transport behaviors [60–64], which can qualitatively distinguish the three different zones. We consider the conductivity σ based on the Kubo formula in the

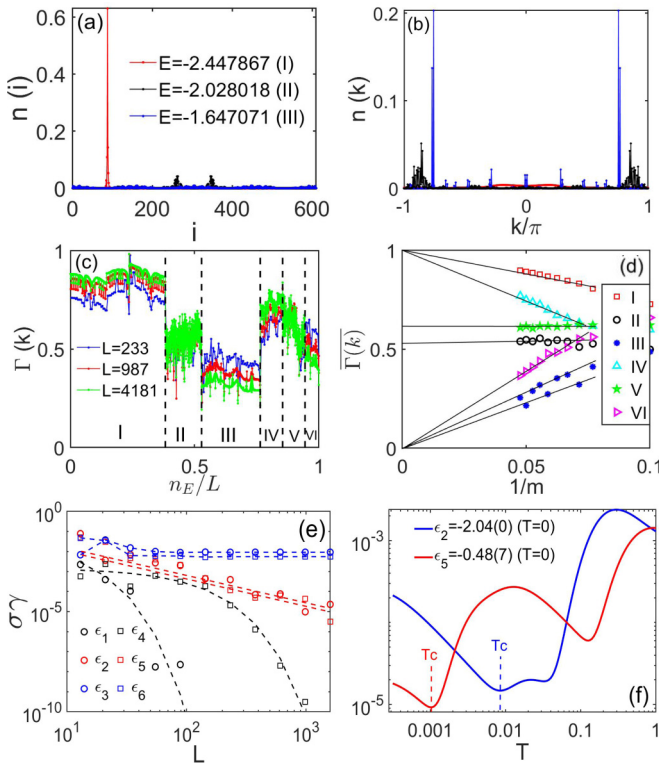


FIG. 4. Typical distribution of the eigenstates in zones I (localized zone), II (critical zone), and III (extended zone) in (a) real space and (b) momentum space. (c) Fractal dimension Γ in momentum space for each eigenstate at three different sizes. (d) $\overline{\Gamma(k)}$ as a function of $1/m$ for different zones, where m are the Fibonacci indices. (e) $\sigma\gamma$ versus L at zero temperature. The Fermi surfaces ϵ_{1-6} in zones I–VI are chosen at $-2.67(4)$, $-2.07(8)$, $-1.79(8)$, $-0.57(7)$, $-0.48(8)$, and $-0.45(7)$, respectively. (f) $\sigma\gamma$ versus temperature with $\alpha = 55/89$. Fermi surfaces in zones II and V are chosen at $\epsilon_2 = -2.04(0)$ and $\epsilon_5 = -0.48(7)$, respectively. Other parameters are $t_{so} = 0.5$, $\lambda = 1/3$, and $M_Z = 1.5$.

dissipationless limit $\gamma \rightarrow 0$ [65,66],

$$\sigma = \frac{1}{2\gamma h} \int dk \sum_b \left(-\frac{df_{FD}[E_b(k) - \mu]}{dE_b(k)} \right) \left(\frac{dE_b(k)}{dk} \right)^2, \quad (6)$$

where f_{FD} is the Fermi-Dirac distribution, E_b is the energy of the b th band, μ is the chemical potential, and γ is the scattering rate [67] assumed to be momentum and band independent. Figure 4(e) shows the conductivity in the zero temperature. We see that for the Fermi surface in the extended zones, the conductivity is independent of system size ($\sigma \sim L^0$), while in the localized zones, conductivity decreases exponentially with the system size ($\sigma \sim e^{-L}$). The conductivity in the critical zones decays in a power-law fashion ($\sigma \sim L^{-p}$, where p is a parameter). The different scaling behaviors of the conductance through varying the Fermi energy clearly show the different types of MEs. With increasing the temperature, the transport behaviors of the critical zones II and V are shown in Fig. 4(f). The transport behavior is more sensitive to temperatures when the distance between the Fermi surface (labeled as ϵ_F) and the minimum value of the above neighbor

extended zone (labeled as E_{\min}^e) is smaller. There is a temperature T_c [$T_c \propto (E_{\min}^e - \epsilon_F)/k_b$, with k_b being the Boltzmann's constant] corresponding to that of the transport effect of the particles that enter the extended zones that becomes nonignorable and thus the conductivity rapidly increases. T_c for zone V is smaller, indicating that both its energy range and the gap between zones V and VI are narrower. To conclude, this phase shows the abundant and different transport features.

Proposal of experimental realization. Here we propose to realize the Hamiltonian (1) in cold atoms by employing the optical Raman lattice scheme. We choose two hyperfine states $|F, m_F\rangle$ and $|F', m'_F\rangle$ to construct the spin-1/2 system, apply a standard spin-independent lattice potential to generate spin-conserved hopping term (H_t), and a Raman coupling potential to induce spin-flip hopping term (H_{SOC}) [17,51–54]. The incommensurate potential term (H_Z) can be generated from scalar and vector potentials induced by two counterpropagating lights with proper polarizations. The realized Hamiltonian reads [57]

$$H = \left[\frac{k_z^2}{2m} + V_1(z) + \lambda V_2 \right] \otimes \mathbb{1} + \mathcal{M}(z)\sigma_x + \left[V_2(z) + \frac{\delta}{2} \right] \sigma_z, \quad (7)$$

where $V_1(z) = V_p \cos^2(k_1 z)$ is the primary lattice, $V_2(z) = \frac{V_s}{2} \cos(2k_2 z + \phi)$ denotes the secondary spin-dependent weak lattice, giving an incommensurate Zeeman potential with the irrational number $\alpha = k_2/k_1$, $\mathcal{M}(z) = M_0 \cos(k_1 z)$ is the Raman coupling potential, and δ is the two-photon detuning. In the SM [57], we show that this continuous Hamiltonian (7) indeed leads to the model Hamiltonian described by Eq. (1).

Here we mainly discuss the key parameter λ . For chosen magnetic quantum numbers m_F, m'_F , λ has a minimal value λ_{\min} when the polarization is mutually perpendicular [57]. In contrast, if the two lights have the same and linear polarization, the incommensurate lattice becomes fully spin independent, corresponding to $\lambda \rightarrow \infty$. Hence λ can vary within the range $\lambda_{\min} \leq \lambda < \infty$ by tuning the light polarization. We consider the mutually perpendicular case, i.e., $\lambda = \lambda_{\min}$, and obtain [57]

$$\lambda_{\min} = \frac{g_F m_F + g_{F'} m'_F}{g_F m_F - g_{F'} m'_F}, \quad (8)$$

where g_F ($g_{F'}$) is the Landé factor for the F (F') hyperfine states. In particular, when $g_F = -g_{F'}$, the result reduces to $\lambda_{\min} = (m_F - m_{F'})/(m_F + m_{F'})$. For example, when using ^{87}Rb bosons to realize the Hamiltonian, one can select $|\uparrow\rangle = |F=2, m_F=-2\rangle$ and $|\downarrow\rangle = |1, -1\rangle$, which gives $\lambda = \lambda_{\min} = 1/3$.

Discussion and conclusion. We have predicted a quantum phase with coexisting localized, extended, and critical zones in a quasiperiodic optical Raman lattice model, which is of high experimental feasibility, and uncovered the underlying mechanism to induce this phase. We introduce the extended-state fraction N_e/N , critical-state fraction N_c/N , and localized-state fraction N_l/N to distinguish the different characteristic zones. The fractal dimensions of extended, critical, and localized states exhibit sharp contrast in size dependence, from which the energy windows and number of states of the

different zones can be determined. Accordingly, this quantum phase can be detected in experiment by measuring the momentum distribution of eigenstates and transport behaviors. Finally, we proposed and studied in detail the experimental realization of the current prediction with ultracold bosons and fermions.

This work adds another family member to the fundamental phases in disordered systems, enriches the localization phenomena, and extends the concept of mobility edges, with many interesting issues deserving further in-depth study. In particular, whether the three different zones are stable when adding finite interactions; namely, is there a correlated quantum phase with coexisting many-body localized, critical, and ergodic zones? Further, can a similar quantum phase exist in

the higher dimensions and in real materials? These issues are fundamentally important and should be explored in following studies.

Acknowledgments. This work is supported by the National Key Research and Development Program of China (Grant No. 2021YFA1400900), the National Natural Science Foundation of China (Grants No. 11825401 and No. 12104205), and the Open Project of Shenzhen Institute of Quantum Science and Engineering (Grant No. SIQSE202003). L.Z. acknowledges support from the startup grant of Huazhong University of Science and Technology (Grant No. 3004012191). W.S. is supported by the Key-Area Research and Development Program of Guangdong Province (Grants No. 2020B0303010001 and No. 2019ZT08X324).

-
- [1] P. W. Anderson, Absence of diffusion in certain random lattices, *Phys. Rev.* **109**, 1492 (1958).
- [2] F. Evers and A. D. Mirlin, Anderson transitions, *Rev. Mod. Phys.* **80**, 1355 (2008).
- [3] P. A. Lee and T. V. Ramakrishnan, Disordered electronic systems, *Rev. Mod. Phys.* **57**, 287 (1985).
- [4] B. Kramer and A. MacKinnon, Localization: Theory and experiment, *Rep. Prog. Phys.* **56**, 1469 (1993).
- [5] S. Aubry and G. André, Analyticity breaking and Anderson localization in incommensurate lattices, *Ann. Israel Phys. Soc.* **3**, 133 (1980).
- [6] S. Das Sarma, S. He, and X. C. Xie, Mobility Edge in a Model One-Dimensional Potential, *Phys. Rev. Lett.* **61**, 2144 (1988).
- [7] J. Biddle, B. Wang, D. J. Priour, Jr., and S. Das Sarma, Localization in one-dimensional incommensurate lattices beyond the Aubry-André model, *Phys. Rev. A* **80**, 021603(R) (2009).
- [8] J. Biddle and S. Das Sarma, Predicted Mobility Edges in One-Dimensional Incommensurate Optical Lattices: An Exactly Solvable Model of Anderson Localization, *Phys. Rev. Lett.* **104**, 070601 (2010).
- [9] S. Ganeshan, J. H. Pixley, and S. Das Sarma, Nearest Neighbor Tight Binding Models with an Exact Mobility Edge in One Dimension, *Phys. Rev. Lett.* **114**, 146601 (2015).
- [10] X. Deng, S. Ray, S. Sinha, G. V. Shlyapnikov, and L. Santos, One-Dimensional Quasicrystals with Power-Law Hopping, *Phys. Rev. Lett.* **123**, 025301 (2019).
- [11] M. Saha, S. K. Maiti, and A. Purkayastha, Anomalous transport through algebraically localized states in one dimension, *Phys. Rev. B* **100**, 174201 (2019).
- [12] X. Li, X. Li, and S. Das Sarma, Mobility edges in one dimensional bichromatic incommensurate potentials, *Phys. Rev. B* **96**, 085119 (2017).
- [13] H. Yao, H. Khoudli, L. Bresque, and L. Sanchez-Palencia, Critical Behavior and Fractality in Shallow One-Dimensional Quasiperiodic Potentials, *Phys. Rev. Lett.* **123**, 070405 (2019).
- [14] Y. Wang, X. Xia, L. Zhang, H. Yao, S. Chen, J. You, Q. Zhou, and X.-J. Liu, One Dimensional Quasiperiodic Mosaic Lattice with Exact Mobility Edges, *Phys. Rev. Lett.* **125**, 196604 (2020).
- [15] X. Li, J. H. Pixley, D.-L. Deng, S. Ganeshan, and S. Das Sarma, Quantum nonergodicity and fermion localization in a system with a single-particle mobility edge, *Phys. Rev. B* **93**, 184204 (2016).
- [16] T. Liu, X. Xia, S. Longhi, and L. Sanchez-Palencia, Anomalous mobility edges in one-dimensional quasiperiodic models, *SciPost Phys.* **12**, 027 (2022).
- [17] Y. Wang, L. Zhang, S. Niu, D. Yu, and X.-J. Liu, Realization and Detection of Nonergodic Critical Phases in an Optical Raman Lattice, *Phys. Rev. Lett.* **125**, 073204 (2020).
- [18] D. J. Thouless, Electrons in disordered systems and the theory of localization, *Phys. Rep.* **13**, 93 (1974).
- [19] E. Abrahams, P. W. Anderson, D. C. Licciardello, and T. V. Ramakrishnan, Scaling Theory of Localization: Absence of Quantum Diffusion in Two Dimensions, *Phys. Rev. Lett.* **42**, 673 (1979).
- [20] G. Roati, C. D'Errico, L. Fallani, M. Fattori, C. Fort, M. Zaccanti, G. Modugno, M. Modugno, and M. Inguscio, Anderson localization of a non-interacting Bose-Einstein condensate, *Nature (London)* **453**, 895 (2008).
- [21] H. P. Lüschen, S. Scherg, T. Kohlert, M. Schreiber, P. Bordia, X. Li, S. D. Sarma, and I. Bloch, Single-Particle Mobility Edge in a One-Dimensional Quasiperiodic Optical Lattice, *Phys. Rev. Lett.* **120**, 160404 (2018).
- [22] F. A. An, E. J. Meier, and B. Gadway, Engineering a Flux-Dependent Mobility Edge in Disordered Zigzag Chains, *Phys. Rev. X* **8**, 031045 (2018).
- [23] F. A. An, K. Padavić, E. J. Meier, S. Hegde, S. Ganeshan, J. H. Pixley, S. Vishveshwara, and B. Gadway, Interactions and Mobility Edges: Observing the Generalized Aubry-André Model, *Phys. Rev. Lett.* **126**, 040603 (2021).
- [24] Y. Hatsugai and M. Kohmoto, Energy spectrum and the quantum Hall effect on the square lattice with next-nearest-neighbor hopping, *Phys. Rev. B* **42**, 8282 (1990).
- [25] Y. Takada, K. Ino, and M. Yamanaka, Statistics of spectra for critical quantum chaos in one-dimensional quasiperiodic systems, *Phys. Rev. E* **70**, 066203 (2004).
- [26] F. Liu, S. Ghosh, and Y. D. Chong, Localization and adiabatic pumping in a generalized Aubry-André-Harper model, *Phys. Rev. B* **91**, 014108 (2015).
- [27] J. Wang, X.-J. Liu, X. Gao, and H. Hu, Phase diagram of a non-Abelian Aubry-André-Harper model with p-wave superfluidity, *Phys. Rev. B* **93**, 104504 (2016).
- [28] V. E. Kravtsov, I. M. Khaymovich, E. Cuevas, and M. Amini, A random matrix model with localization and ergodic transitions, *New J. Phys.* **17**, 122002 (2015).

- [29] V. E. Kravtsov, B. L. Altshuler, and L. B. Ioffe, Non-ergodic delocalized phase in Anderson model on Bethe lattice and regular graph, *Ann. Phys. (NY)* **389**, 148 (2018).
- [30] S. Whitlock, H. Wildhagen, H. Weimer, and M. Weidemüller, Diffusive to Nonergodic Dipolar Transport in a Dissipative Atomic Medium, *Phys. Rev. Lett.* **123**, 213606 (2019).
- [31] A. K. Das, and A. Ghosh, Nonergodic extended states in the β ensemble, *Phys. Rev. E* **105**, 054121 (2022).
- [32] T. T. Geisel and G. Petschel, New Class of Level Statistics in Quantum Systems with Unbounded Diffusion, *Phys. Rev. Lett.* **66**, 1651 (1991).
- [33] S. Y. Jitomirskaya, Metal-insulator transition for the almost mathieu operator, *Ann. Math.* **3**, 150 (1999).
- [34] In mathematical terminology, the energy spectrum is absolutely continuous and singular continuous in extended and critical phases, respectively. The localized system possesses a point spectrum [33].
- [35] T. C. Halsey, M. H. Jensen, L. P. Kadanoff, I. Procaccia, and B. I. Shraiman, Fractal measures and their singularities: The characterization of strange sets, *Phys. Rev. A* **33**, 1141 (1986).
- [36] A. D. Mirlin, Y. V. Fyodorov, A. Mildenerger, and F. Evers, Exact Relations between Multifractal Exponents at the Anderson Transition, *Phys. Rev. Lett.* **97**, 046803 (2006).
- [37] H. Hiramoto and S. Abe, Dynamics of an electron in quasiperiodic systems. II. Harper's model, *J. Phys. Soc. Jpn.* **57**, 1365 (1988).
- [38] R. Ketzmerick, K. Kruse, S. Kraut, and T. Geisel, What Determines the Spreading of a Wave Packet? *Phys. Rev. Lett.* **79**, 1959 (1997).
- [39] Y. Wang, C. Cheng, X.-J. Liu, and D. Yu, Many-Body Critical Phase: Extended and Nonthermal, *Phys. Rev. Lett.* **126**, 080602 (2021).
- [40] T. Xiao, D. Xie, Z. Dong, T. Chen, W. Yi, and B. Yan, Observation of topological phase with critical localization in a quasi-periodic lattice, *Sci. Bull.* **66**, 2175 (2021).
- [41] A. Pal and D. A. Huse, Many-body localization phase transition, *Phys. Rev. B* **82**, 174411 (2010).
- [42] R. Nandkishore and D. A. Huse, Many-body localization and thermalization in quantum statistical mechanics, *Annu. Rev. Condens. Matter Phys.* **6**, 15 (2015).
- [43] A. Purkayastha, S. Sanyal, A. Dhar, and M. Kulkarni, Anomalous transport in the Aubry-André-Harper model in isolated and open systems, *Phys. Rev. B* **97**, 174206 (2018).
- [44] D. A. Abanin, E. Altman, I. Bloch, and M. Serbyn, Colloquium: Many-body localization, thermalization, and entanglement, *Rev. Mod. Phys.* **91**, 021001 (2019).
- [45] H. Fritzsche, A general expression for the thermoelectric power, *Solid State Commun.* **9**, 1813 (1971).
- [46] U. Sivan and Y. Imry, Multichannel Landauer formula for thermoelectric transport with application to the thermopower near the mobility edge, *Phys. Rev. B* **33**, 551 (1986).
- [47] G. Benenti, G. Casati, K. Saito, and R. S. Whitney, Fundamental aspects of steady-state conversion of heat to work at the nanoscale, *Phys. Rep.* **694**, 1 (2017).
- [48] R. Whitney, Most Efficient Quantum Thermoelectric at Finite Power Output, *Phys. Rev. Lett.* **112**, 130601 (2014).
- [49] K. Yamamoto, A. Aharony, O. Entin-Wohlman, and N. Hatano, Thermoelectricity near Anderson localization transitions, *Phys. Rev. B* **96**, 155201 (2017).
- [50] C. Chiaracane, M. T. Mitchison, A. Purkayastha, G. Haack, and J. Goold, Quasiperiodic quantum heat engines with a mobility edge, *Phys. Rev. Res.* **2**, 013093 (2020).
- [51] X.-J. Liu, Z.-X. Liu, and M. Cheng, Manipulating Topological Edge Spins in a One-Dimensional Optical Lattice, *Phys. Rev. Lett.* **110**, 076401 (2013).
- [52] B. Song, L. Zhang, C. He, T. F. J. Poon, E. Hajiyeve, S. Zhang, X.-J. Liu, and G.-B. Jo, Observation of symmetry-protected topological band with ultracold fermions, *Sci. Adv.* **4**, eaao4748 (2018).
- [53] B.-Z. Wang, Y.-H. Lu, W. Sun, S. Chen, Y. Deng, and X.-J. Liu, Dirac-, Rashba-, and Weyl-type spin-orbit couplings: Toward experimental realization in ultracold atoms, *Phys. Rev. A* **97**, 011605(R) (2018).
- [54] L. Zhang and X.-J. Liu, Spin orbit coupling and topological phases for ultracold atoms, [arXiv:1806.05628](https://arxiv.org/abs/1806.05628).
- [55] M. Kohmoto, Metal-Insulator Transition and Scaling for Incommensurate Systems, *Phys. Rev. Lett.* **51**, 1198 (1983).
- [56] Fibonacci numbers are defined recursively by $F_{m+1} = F_m + F_{m-1}$ with $F_0 = F_1 = 1$.
- [57] See Supplemental Material at <http://link.aps.org/supplemental/10.1103/PhysRevB.106.L140203> for details on (I) a brief introduction to nonergodic critical phase, (II) more situations of λ , (III) an underlying mechanism for the occurrence of the coexisting quantum phase, (IV) the finite size analysis for $N_e/N, N_c/N, N_l/N$ and the scaling index, and (V) the experimental realization. The Supplemental Material includes Refs. [5,7,8,10–13,15,17,28–31,51–53,68,69].
- [58] In our work, we provide two different approaches to determine the number of eigenstates in different zones. The first is obtained in three steps: (i) to calculate the fractal dimensions of all eigenstates for different sizes, (ii) to determine the energy windows of different zones, and (iii) to numerically compute the number of eigenstates in these different energy windows, giving $N_e/N, N_c/N, N_l/N$. Another approach is to use the ratio of the index of energy mode n_E to L as the horizontal axis, instead of the eigenvalue E , which can also directly determine $N_e/N, N_c/N, N_l/N$. From the first approach, one can obtain the eigenenergy distribution and energy range of different zones, but sometimes one needs to enlarge some zones of difficult judgment to make the zone division more precise. From the second approach, one can directly obtain $N_e/N, N_c/N, N_l/N$, because there exists the sudden change between different zones [see Fig. 3(c)]; then one can easily obtain the energy gap of different zones numerically. Combining the two approaches, one can obtain the complete information of energy spectrum and eigenstates. The two approaches can be applied to other generic models.
- [59] If a zone includes the mobility edge separating extended and localized states, the average Γ does not tend to 0 or 1, but they typically monotonously increase or decrease with increasing the system size, depending on the relative number of extended and localized states, which is different from the critical zone. One can detect the average Γ in any two small subzones to further distinguish them. If the two small subzones show the same scaling behavior with the zone, this zone is critical. If at least one shows the same scaling behavior with the extended or localized zone, this zone has mobility edge.
- [60] C.-C. Chien, S. Peotta, and M. D. Ventura, Quantum transport in ultracold atoms, *Nat. Phys.* **11**, 998 (2015).

- [61] J.-P. Brantut, J. Meineke, D. Stadler, S. Krinner, and T. Esslinger, Conduction of ultracold fermions through a mesoscopic channel, *Science* **337**, 1069 (2012).
- [62] J.-P. Brantut, C. Grenier, J. Meineke, D. Stadler, S. Krinner, C. Kollath, T. Esslinger, and A. Georges, A thermoelectric heat engine with ultracold atoms, *Science* **342**, 713 (2013).
- [63] S. Krinner, D. Stadler, J. Meineke, J.-P. Brantut, and T. Esslinger, Superfluidity with Disorder in a Thin Film of Quantum Gas, *Phys. Rev. Lett.* **110**, 100601 (2013).
- [64] S. Krinner, D. Stadler, D. Husmann, J.-P. Brantut, and T. Esslinger, Observation of quantized conductance in neutral matter, *Nature (London)* **517**, 64 (2015).
- [65] G. D. Mahan, *Many-Particle Physics* (Kluwer Academic/Plenum, New York, 2000).
- [66] J. Mitscherling, Longitudinal and anomalous Hall conductivity of a general two-band model, *Phys. Rev. B* **102**, 165151 (2020).
- [67] The value of γ depends on concrete systems and can be determined in experiments.
- [68] K. Wen, Z. Meng, L. Wang, L. Chen, L. Huang, P. Wang, and J. Zhang, Experimental study of tune-out wavelengths for spin-dependent optical lattice in ^{87}Rb Bose-Einstein condensation, *J. Opt. Soc. Am. B* **38**, 3269 (2021).
- [69] D. McKay and B. DeMarco, Thermometry with spin-dependent lattices, *New J. Phys.* **12**, 055013 (2010).